



Carbon Honeycomb High Capacity Storage for Gaseous and Liquid Species

Nina V. Krainyukova¹ and Evgeniy N. Zubarev²

¹*B. Verkin Institute for Low Temperature Physics and Engineering of the National Academy of Sciences of Ukraine, 47 Lenin Avenue, 61103 Kharkiv, Ukraine*

²*National Technical University “Kharkiv Polytechnical Institute,” 21 Frunze-Street, 61002 Kharkiv, Ukraine*

(Received 14 June 2015; published 5 February 2016)

We report an exceptionally stable honeycomb carbon allotrope obtained by deposition of vacuum-sublimated graphite. The allotrope structures are derived from our low temperature electron diffraction and electron microscopy data. These structures can be both periodic and random and are built exclusively from sp^2 -bonded carbon atoms, and may be considered as three-dimensional graphene. They demonstrate high levels of physical absorption of various gases unattainable in other carbon forms such as fullerenes or nanotubes. These honeycomb structures can be used not only for storage of various gases and liquids but also as a matrix for new composites.

DOI: 10.1103/PhysRevLett.116.055501

The carbon allotropes such as fullerenes [1], nanotubes [2], schwarzite forms [3,4], graphene [5], carbon foams [6–9], sp^1 carbon, or carbon atomic wires [10] discovered within the past quarter of a century exhibit many unique properties and have numerous applications in science and industry. It was proposed [3] that, depending on the growth rate, the arc-discharge sublimation of carbon from graphite in vacuum may result in fullerenes at slow growth and schwarzite forms [3,4] at fast growth. In this study we show that if the arc discharge is avoided and only carbon sublimation in vacuum is allowed, unique structural forms of carbon with high absorption ability emerge (Fig. 1).

In our synthesis procedure carbon was evaporated in vacuum from thin carbon rods [11] heated by electric current. Carbon films with thickness $\sim 80\text{--}100$ Å were obtained and analyzed by means of transmission electron microscopy (TEM) and low temperature high energy electron diffraction.

High resolution TEM images [Fig. 2(a)] demonstrate that carbon films are pierced by numerous channels explaining the high absorption ability of these structures reported previously [12]. Such channels form irregular triangular lattices based on links between axes of channels. Most of these channels are nearly normal to the film surfaces, but a smaller amount is tilted with respect to the surface.

The high absorption ability of our carbon films was revealed when gaseous krypton, xenon [12], and carbon dioxide were deposited on carbon substrates inside the helium cryostat in the electron diffraction setup at 23, 40, and 78 K, respectively. At first, good quality thin solid polycrystalline films with distinct diffraction peaks are formed [see Fig. 3(a)]. But when they are gradually heated and kept slightly below the characteristic sublimation points (42, 59, and 88 K for considered Kr, Xe, and CO₂, respectively), the strong diffraction peaks corresponding to a polycrystalline state disappear, but distinct residual

signals remain. These signals are still observed at temperatures far above the sublimation points owing to physical absorption of gases with strong bonding in the carbon matrix [Fig. 3(b)]. The difference in intensities is mainly due to the scattering abilities of these substances (highest for Xe and lowest for CO₂) but not to their levels of absorption which is of a comparable value $\sim 4\text{--}6\%$ in an atomic count with respect to carbon atoms in a substrate.

As we described in detail previously [12–14], for precise analysis of diffraction patterns, the experimental intensities $I_{\text{exp}}(S)$ (Fig. 3) are compared with calculated intensities:

$$I_{\text{calc}}(S) = \exp(-\langle u^2 \rangle S^2) f^2 \left[1/(1-t) + \sum_k w_k I_{\text{calc},k}(S) \right]. \quad (1)$$

Here, $\langle u^2 \rangle$ are the mean-square atomic displacements, f is the atomic scattering factor for electrons, w_k are the varied probabilities of the presence of a structural fragment k composed of N_k atoms, and



FIG. 1. The proposed periodic and random honeycomb carbon structures.

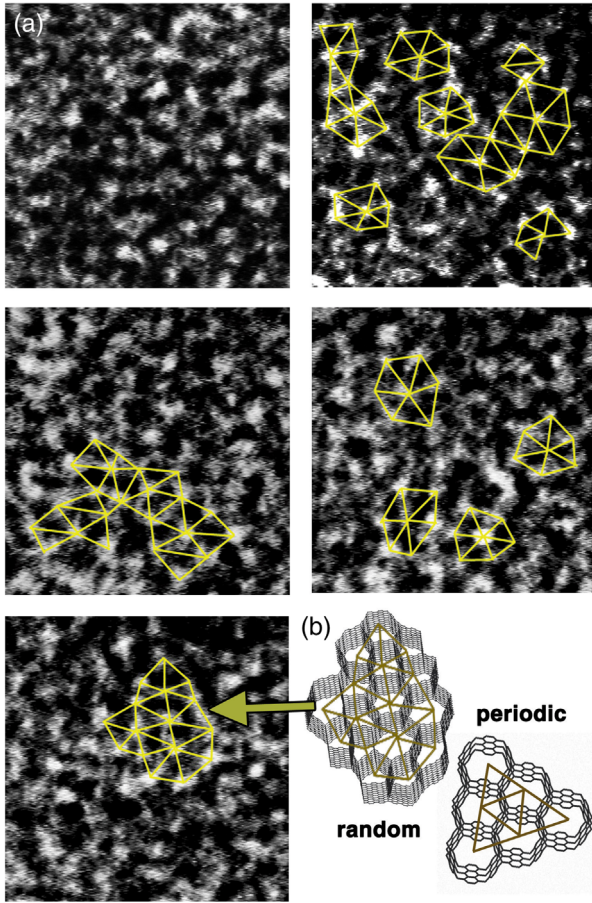


FIG. 2. (a) TEM images (positive, $120 \times 120 \text{ \AA}$ each) of a carbon film, exhibiting numerous channels that are mostly perpendicular to the surface. The channels form irregular triangular lattices with shown example links between axes of channels. One can proceed with such links to other channels. (b) Our reconstruction of the particular channels (marked on the left) via the proposed random honeycomb structure. The periodic triangular lattice is also shown.

$$I_{\text{calc},k}(S) = (2/N_k) \left[\sum_{m>n} \sin(Sr_{mn})/Sr_{mn} \right]_k \quad (2)$$

is the Debye formula, where r_{mn} is the distance between a pair of atoms in a structural fragment k and $\sum_k w_k = 1$. The value $t \sim 0.25$ (in contrast with isolated clusters [13]) characterizes a fraction of atoms belonging to different fragments whose oscillating terms with $I_{\text{calc},k}(S)$ [Eq. (2)] mutually cancel each other in $I_{\text{calc}}(S)$ [Eq. (1)], giving a contribution only in the monotonic term $\sim f^2$. In the fitting of the calculated diffraction intensities with respect to experimental ones, we minimized the reliability factor

$$R = \sum_S |I_{\text{exp}} - I_{\text{calc}}| / \sum_S (I_{\text{exp}} + I_{\text{calc}}) \quad (3)$$

with respect to w_k ; here, the summation over S is performed with the step 0.02 \AA^{-1} . Numerous structures including

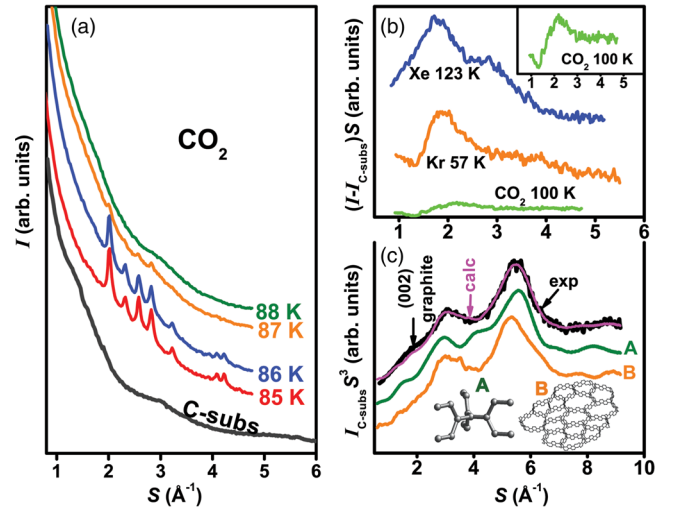


FIG. 3. (a) The electron diffraction intensities I for condensed CO_2 vs the scattering wave vector $S = 4\pi \sin(\theta/\lambda)$. Here, 2θ is the scattering angle and λ is the de Broglie wavelength of the electrons. The diffraction curve for the carbon substrate (C-subs) is also shown. (b) The electron diffraction intensities I for Xe, Kr, and CO_2 absorbed in the carbon substrate with the carbon substrate contribution $I_{\text{C-subs}}$ subtracted. The dependence for absorbed CO_2 is also shown in an inset to clarify its character. (c) Experimental (exp, recorded at 8 K) and best fit calculated [calc, see Eq. (1)] diffraction intensities for the carbon substrate. The calculated diffractograms for two dominant structures A and B are shown below. The diffraction curves in (a) and (c) are shifted vertically for clarity and ease of comparison.

graphite, fullerenes, schwarzites, and nanotubes (both single and intersecting, similar to those existing in carbon foam [8,9]) and their fragments were tested in order to describe the S dependence of the diffraction intensities $I_{\text{exp}}(S)$ in carbon films [Fig. 3(c)]. We have found that different sized graphite fragments are bad candidates for such description. This was confirmed by the obviously weakened (002) diffraction peak characteristic of the spacing between graphite basal planes [Fig. 3(c)]. Carbon nanotubes of some specific forms and sizes were better candidates, but their probable appearance could have a special origin discussed below. The obtained data were scrutinized to find a better fit.

As it was proposed previously [4,15], we have calculated the reduced density function

$$G(r) = (2/\pi) \int_0^{S_{\text{max}}} S \{ [I_{\text{exp}}(S) - Af^2]/Af^2 \} D(S) \times \sin(Sr) dS, \quad (4)$$

applying the Fourier-sine transformation with respect to the experimental diffraction patterns $I_{\text{exp}}(S)$ from carbon films; here, A is proportional to the total amount of the scattering centers and the incident beam intensity and

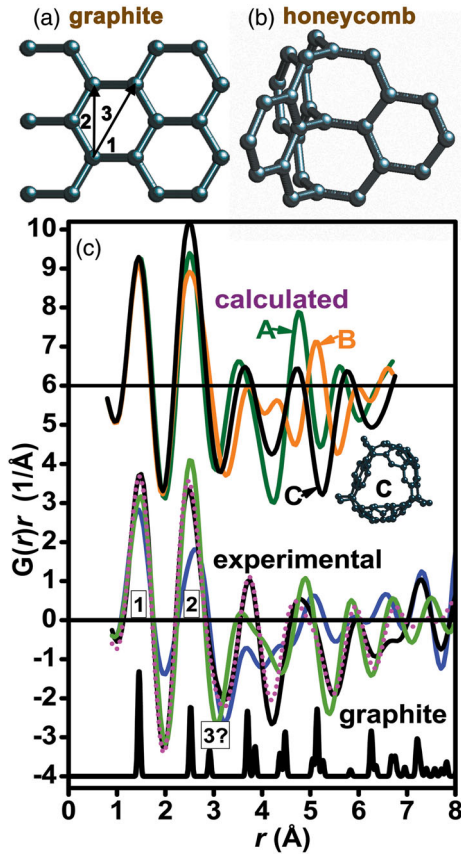


FIG. 4. Structural elements of (a) graphite and (b) proposed honeycomb structures. (c) The experimental density functions obtained for four different carbon films are compared with calculated curves based on $I_{\text{calc}}(S)$ [Eq. (1)] for three dominant model structures A, B, and C [11], as well as with $\rho(r)$ of graphite in arbitrary units. The lower and upper curves in (c) are shifted vertically.

$$D(S) = \text{sinc}(S/S_{\text{max}}) \quad (5)$$

is the damping function. A better form for the function $G(r)$ is $G(r)r$ [Fig. 4(c)], since

$$G(r)r = 4\pi r^2[\rho(r) - \rho_0] \quad (6)$$

characterizes the deviation of the number of atoms from their average amount at a distance r ; here, $\rho(r)$ and ρ_0 are the local and average densities, respectively. In Fig. 4(c) we show the results for four samples.

A simple geometric consideration of the first $r_1 = 1.44 \pm 0.02$ Å and second $r_2 = 2.49 \pm 0.03$ Å nearest neighbor distances [Fig. 4(c)] yields an angle α between the two bonds $\alpha = 119.7 \pm 0.3^\circ$ leading to an immediate conclusion that sp^2 bonding is absolutely dominant. In contrast, one should expect a distinct tendency towards $\alpha = 109.5^\circ$ for sp^3 bonding. One important observation concerning the third neighbor is its damped contribution in the density function. Several structures were considered

to find an explanation of this fact, but had to be rejected, in particular owing to the mismatch between the experimentally determined and calculated carbon densities, as well as possible levels of absorption. The details are given below. We thus switched to the structural element shown in Fig. 4(b), where the third neighbor is completely absent for a fraction of atoms. We show the calculated diffraction pattern for the symmetrically truncated form with 16 atoms as A in Fig. 3(c). The contribution of A into $I_{\text{calc}}(S)$ is $w_k \sim 0.4$.

To get more information about our structures, we have also calculated the average densities ρ_0 . We equated the integral

$$\int [G(r) + 4\pi r \rho_0] r dr \quad (7)$$

over the first peak to exactly three (the number of nearest neighbors) as expected for sp^2 bonding. We obtained $\rho_0 = 0.077$ atoms/Å³ (or 1.53 g/cc) with high reproducibility. The close value $\rho_0 = 1.4 \pm 0.1$ g/cc was obtained when we used small-angle x-ray reflective diffraction for our carbon films. This fact rejects our initial idea about schwarzites [3,4], because all previously known forms had lower ρ_0 . The direct observations of some schwarzites [16], which were even several times less dense compared with the above predictions [4], further confirmed our assumption that our structure is different.

In order to construct reliable carbon structures consistent with the observed absorption levels, we should take into account that the equilibrium distances between Kr or Xe atoms and a graphitic sheet are 3.19 and 3.34 Å, respectively [17], and these distances should be used as radii of spaces where Kr or Xe atoms can be placed.

The TEM images in Fig. 2(a) look similar to the pictures from ropes of nanotubes [18]. By comparing densities of probable nanotubes given their specific sizes with available levels of physical absorption, we concluded that the possible absorption in tubes is about twice as low as that experimentally observed. Additionally, our films with thickness $\sim 80 - 100$ Å were exceptionally stable and did not undergo any degradation when kept in vacuum for at least several months. Such stability is hardly possible for short ropes of tubes. In ropes of tubes empty spaces are separated by double walls belonging to two nearest neighbor tubes. Therefore, we should find structures with a single wall between “cages” for absorbed atoms. The images in Fig. 2(a) give us distances between channels. We return to the model fragment shown in Fig. 4(b) and expand this fragment with the specific intersection of graphitic planes in a regular way, resulting in a periodic honeycomb structure as shown in Figs. 1 and 2(b). Here, three flat graphitic sheets, which are known to be the most stable carbon form with sp^2 bonding, are joined together at an angle 120° between two sheets along a straight line. In

contrast with carbon foams [6,7], the sp^2 bonding is kept along such lines, which results in some kind of 3D graphene. We expect some advantage of our structural model as compared with models with sp^3 junction lines [6,7] owing to the reduction of the number of atoms in positions that correspond to the strong van der Waals repulsion at distances much shorter than the equilibrium distance ~ 3.5 Å. The distance is derived from a lattice of graphite with the interaction between basal planes due to the van der Waals forces. Variations of the distance between the nearest junction lines $(2.5 + 1.5n)r_{\text{NN}}$, where n is an integer and $r_{\text{NN}} = r_1 = 1.44$ Å is the nearest neighbor distance in a graphitic sheet, enable us to make diverse structures with thinner or wider channels, or random structures. Such a random structure is reconstructed in Fig. 1 (random) and Fig. 2(b) based on an electron microscopy image. Its truncated form was used in our analysis of diffraction as structure B in Fig. 3(c), corresponding to $w_k \sim 0.15$, along with some other fragments of the found structures [11]. The most important elements of our structure are the junction lines formed by sp^2 -bonded carbon atoms, while sizes and configurations of channels can vary. The best coincidence with the experimentally observed density ρ_0 is attained for $n = 1$, $\rho_0 = 0.074$ atoms/Å³ (or ~ 1.48 g/cc). The structure with $n = 1$ could also result in the necessary levels of absorption. The relevant illustrations are shown in Fig. 5(a).

We emphasize that many gaseous or liquid species with their own interatomic or intermolecular interactions that are weaker than the interaction with carbon walls will stay once absorbed in our honeycomb structure far above the temperature of evaporation in their free forms. The absorption

capacities can be regulated by the value n . For the considered $n = 1$, we may expect a single atomic or molecular chain along a honeycomb axis [as in Fig. 5(a)], but for higher n more than one atom can be placed in a plane normal to the axis. In particular, for He and H₂, we could attain the relative densities of absorbed substances with respect to a matrix of ~ 16 and 8 wt%, respectively, for $n = 3$. Physisorbed He and H₂ may hardly be kept in a neutral carbon matrix at high enough temperatures, but the partial ionization of carbon honeycomb by analogy with the fullerenes [19] may increase the binding energy, e.g., for He up to ~ 120 K.

Although nanotubes were rejected as the main structures, we suppose that they may coexist in symbiosis with the honeycomb structures, as shown in Fig. 5(b), especially near the film boundaries, tending to saturate dangling bonds. Fragments of such symbiosis were also included in our analysis of the diffraction data [Fig. 3(c)], and its reliability was confirmed by nonzero $w_k \sim 0.05$ – 0.08 in Eq. (1).

Previously, several attempts were made to associate the structure of “amorphous” carbon either with schwarzite forms [4], if films were grown by the electron beam heating of a graphite target, or with the tetrahedral atomic arrangement [15], in runs of a filtered plasma stream of a vacuum arc on graphite. Both of these methods are different from the specific preparation technique used in our current study. By using magnetron sputtering, i.e., changing the method of film production, we also obtained much denser films with prevailed sp^3 bonding. Hence, the so-called amorphous carbon films obviously have different structures depending on the preparation procedure. In general, the films obtained by evaporation are much less dense as compared with ones produced by sputtering. The difference most plausibly is due to the much higher atomic energy in sputtering as compared to evaporation.

Concerning past observations of absorption, we have found one study that may be relevant to our work. In the early 1970s Venables and Ball [20] monitored a nucleation process when depositing gases on amorphous carbon substrates obtained by evaporation close to the sublimation point. They revealed a noticeable delay between the beginning of deposition and the first appearance of crystallites. Although our procedure is different in that we observed the absorption from initially solid deposited films owing to intensive diffusion below the sublimation point, the time delay in the experiment of Venables and Ball can also be ascribed to possible absorption until all available channels are closed.

The proposed honeycomb structure is the only one among known carbon forms that complies with the whole set of our experimental observations, i.e., the measured absorption levels, densities of carbon films, specific carbon interatomic distances, and angles between bonds, diffraction profiles compared with model calculations, and TEM images with distinct features. This structure is based on the

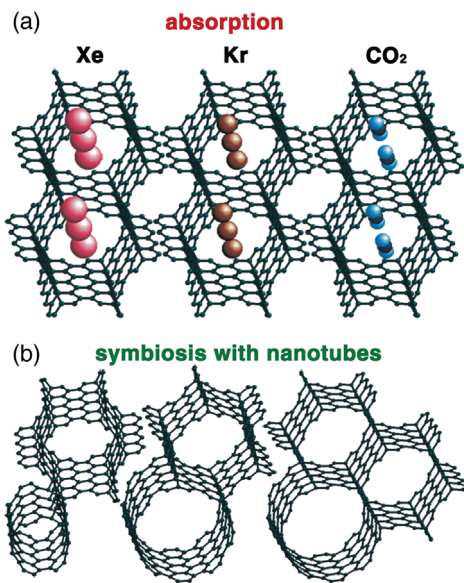


FIG. 5. (a) Examples of gas absorption in honeycomb consistent with observed and estimated absorption levels. (b) Unique symbiosis of the proposed honeycomb structure with nanotubes.

most stable sp^2 carbon configuration and can be considered as 3D graphene. The proposed honeycomb structure is promising not only as high capacity storage with a strong bonding effect, but may also demonstrate unique properties (magnetic, electric, etc.) after being filled with different substances, owing to its one dimensionality along honeycomb axes, or as a unique composite.

The authors thank S. Feodos'ev for helpful discussions.

-
- [1] H. W. Kroto, J. R. Heath, S. C. O'Brien, R. F. Curl, and R. E. Smalley, *Nature (London)* **318**, 162 (1985).
- [2] S. Iijima, *Nature (London)* **354**, 56 (1991).
- [3] T. Lenosky, X. Gonze, M. Teter, and V. Elser, *Nature (London)* **355**, 333 (1992).
- [4] S. J. Townsend, T. J. Lenosky, D. A. Muller, C. S. Nichols, and V. Elser, *Phys. Rev. Lett.* **69**, 921 (1992).
- [5] K. S. Novoselov, A. K. Geim, S. V. Morozov, D. Jiang, Y. Zhang, S. V. Dubonos, I. V. Grigorieva, and A. A. Firsov, *Science* **306**, 666 (2004).
- [6] K. Umemoto, S. Saito, S. Berber, and D. Tománek, *Phys. Rev. B* **64**, 193409 (2001).
- [7] A. Kuc and G. Seifert, *Phys. Rev. B* **74**, 214104 (2006).
- [8] F. Ding, Y. Lin, P. O. Krasnov, and B. I. Yakobson, *J. Chem. Phys.* **127**, 164703 (2007).
- [9] A. K. Singh, J. Lu, R. S. Aga, and B. I. Yakobson, *J. Phys. Chem. C* **115**, 2476 (2011).
- [10] A. Milani, M. Tommasini, V. Russo, A. L. Bassi, A. Lucotti, F. Cataldo, and C. S. Casari, *Beilstein J. Nanotechnol.* **6**, 480 (2015).
- [11] See Supplemental Material at <http://link.aps.org/supplemental/10.1103/PhysRevLett.116.055501> for the carbon film preparation procedure and the full list of structures found in the analysis of diffraction intensities for carbon films.
- [12] N. V. Krainyukova, *Low Temp. Phys.* **35**, 294 (2009).
- [13] V. Kiryukhin, E. P. Bernard, V. V. Khmelenko, R. E. Boltnev, N. V. Krainyukova, and D. M. Lee, *Phys. Rev. Lett.* **98**, 195506 (2007).
- [14] N. V. Krainyukova, R. E. Boltnev, E. P. Bernard, V. V. Khmelenko, D. M. Lee, and V. Kiryukhin, *Phys. Rev. Lett.* **109**, 245505 (2012).
- [15] D. R. McKenzie, D. Muller, and B. A. Pailthorpe, *Phys. Rev. Lett.* **67**, 773 (1991).
- [16] E. Barborini, P. Piseri, and P. Milani, *Appl. Phys. Lett.* **81**, 3359 (2002).
- [17] G. Vidali and M. W. Cole, *Phys. Rev. B* **29**, 6736 (1984).
- [18] A. Thess *et al.*, *Science* **273**, 483 (1996).
- [19] C. Leidlmaier *et al.*, *Phys. Rev. Lett.* **108**, 076101 (2012).
- [20] J. A. Venables and D. J. Ball, *Proc. R. Soc. A* **322**, 331 (1971).